Heliyon 9 (2023) e20049

Contents lists available at ScienceDirect

Heliyon

journal homepage: www.cell.com/heliyon

Evidence of electronic influence in the adsorption of cationic and zwitterionic dyes on zeolites

Elizabeth Von-Kiti [a,*], William Owusu Oduro [a], Maame Adwoa Animpong [a], Kofi Ampomah-Benefo [a], Gloria Boafo-Mensah [a], Bright Kwakye-Awuah [b], Craig Denver Williams [c]

[a] Materials and Manufacturing Division, Council for Scientific and Industrial Research –Institute of Industrial Research (CSIR-IIR), Accra, Ghana
[b] Department of Physics, Kwame Nkrumah University of Science and Technology, Kumasi, Ghana
[c] School of Sciences and Engineering, University of Wolverhampton, Wolverhampton, UK

ARTICLE INFO

Keywords:
Adsorption
Zwitterionic dyes
Freundlich isotherm
Electrostatic and geometric effects
Characterization

ABSTRACT

The adsorption of a cationic dye, Methylene blue (MB), and a zwitterionic dye, 8-Hydroxyquinoline (8-HQ), onto zeolites synthesized from different clays has been investigated. The presence of certain metals and the Si/Al ratio of the parent clay has an overall effect on the type of zeolites produced. Zeolites LTA and FAU Y were obtained using the hydrothermal method. X-ray diffraction and Fourier transform infrared spectroscopy (FTIR) spectral analysis was used to study the adsorption phenomena of the adsorbates on the adsorbents. The adsorption profile of MB (Topological Polar Surface Area (TPSA) 43.9 $Å^2$ and 8-HQ (TPSA 33.1 $Å^2$) compared favourably with a Freundlich isotherm with $R^2 > 0.9$ for all the zeolitic materials synthesized. Adsorption capacities of zeolite FAU was significantly different from zeolite LTA for MB removal. The higher adsorption capacity of zeolite FAU was attributed to geometric effects resulting in greater shrinkage in the inter lattice spacing of zeolite LTA leading to a reduction in surface area. Adsorption of the relatively smaller 8-HQ however, did not show significant difference in the two zeolite types. Surface and structural characterization showed that adsorbates/adsorbents interactions were driven by both geometric (inter lattice spacing which imparts higher surface area of the adsorbent) and electronic (electrostatic repulsions through electron back donation from metals in the zeolitic structure) considerations.

1. Introduction

Several industries generate waste in the form of wastewater which contain toxic compounds, coloured organic contaminants (including dyes) and micro-organisms. Due to the toxic nature of most dyes to plants, aquatic life and the environment, effluents from industries require adequate treatment before discharge [1]. These coloured dyes could either be anionic, cationic or non-ionic. The high solubility of reactive dyes, the most dominant class of dyes used in the textile industry, in water make removal by conventional coagulation and activated sludge processes very difficult [2]. Methylene blue (MB), a cationic dye belonging to the group of xanthene dyes are widely used for the dyeing of paper, cotton, leather and wool in industries. They have applications in the pharmaceutical and

* Corresponding author. Materials and Manufacturing Division, Council for Scientific and Industrial Research –Institute of Industrial Research (CSIR-IIR), Accra, Ghana.
E-mail address: evonkiti@csir-iir.com (E. Von-Kiti).

https://doi.org/10.1016/j.heliyon.2023.e20049
Received 14 April 2023; Received in revised form 8 September 2023; Accepted 9 September 2023
Available online 12 September 2023

cosmetic industries as well. High doses of MB in the body may lead to skin irritations, rapid heartbeat, respiratory problems, nausea, vomiting and abdominal pains [3].

8-hydroxyquinoline (8-HQ), also known as oxine, is an organic compound derived from the heterocycle quinolone. It is used in analytical chemistry for forming stable chelating complexes with many metal cations. In mineral processing, the oxinates acts as collectors through chemisorption on mineral particle surfaces during flotation processes [4]. It also has a role as an antibacterial agent, iron chelator, antiseptic drug and antifungal agrochemical to control grey mold on vines and tomatoes [5,6]. It is corrosive, toxic, irritant and a health hazard. Due to the implications caused by these dyes in the environment, there is the need to remove or reduce their occurrence to a minimum in industrial effluents before discharging them into waterbodies or the environment [7].

Several chemical, physical and biological methods have been developed to remove dyes from the environment. Some of them include adsorption, membrane filtration, electrocoagulation, photochemical decomposition as well as advanced oxidation processes [8].

Adsorption technique which is a surface phenomenon is by far the most versatile, efficient, and economically feasible process that is used for separation and purification and therefore widely used [7,9]. The adsorption probability of dye molecules depends on both the material (chemistry) of the adsorbent and the crystallographic orientation (morphology) of the substances. Studies have reported the use of peat, clay, activated carbon [10] as well as zeolites and metal oxides [2] as some of the most common adsorbent materials. Low cost adsorbents from readily available raw materials have been considered by many researchers. As such the use of clay, municipal solid waste ash and fly ash for the synthesis of zeolites has been studied [11,12].

The crystalline framework of zeolites (microporous materials which have a surface area of about 500–800 m^2/g) with well-defined micro cavities and channels also impacts attractive adsorption properties. The proportion of SiO_2/Al_2O_3 in zeolites influences their physical and chemical properties. The Si/Al ratio is inversely proportional to the cation content and the surface selectivity of the zeolite changes from hydrophilic to hydrophobic with increasing Si/Al ratio [13]. Low silica zeolites have SiO_2/Al_2O_3 mass ratio of 1.18–2.35, SiO_2/Al_2O_3 mass ratio of 3.53–11.76 indicates medium silica zeolites whilst high silica zeolites have a mass ratio greater than 11.76 [14]. Organic molecules (hydrocarbons, oxygen-containing compounds, halogenated derivatives, amines, humic acids, proteins, and lipids) which are too large to penetrate the channels of the zeolites are adsorbed unto its surface [15]. Thus, zeolites can be effective dye removers depending on the topological surface area of the dye molecule. This paper investigates the efficacy of different zeolitic materials with varying Si/Al in the removal of methylene blue a cationic dye with topological polar surface area of 43.9 $Å^2$ and relatively smaller zwitterionic 8-Hydroxyquinoline (33.1 $Å^2$) dyes from water. The adsorptive properties of dyes with varied sizes on the as-synthesized adsorbents mimics the cavities, channels and lattice planes of adsorbents determining the adsorption process.

2. Materials

Clay was sourced locally from Mankessim (MK) and Abonku (AB) in the Central region of Ghana and Anfoega (ANF) in the Volta region of Ghana which notable commercially available clay deposits. Anhydrous grade Sodium hydroxide (NaOH, Analytical grade, Analar, UK) was used as the alkali source for the zeolite synthesis.

Methylene Blue (MB), cationic dye and crystalline 8-hydroxyquinoline (8-HQ), a zwitterionic dye were both sourced from Sigma-Aldrich and used without any further purification. Fig. 1a and b represent the resonance structures of the MB and 8-HQ dyes respectively.

3. Methods

3.1. Zeolite synthesis

The clays were washed to remove any organic matter, dewatered, air dried and pulverised to a powdery form. They were then stored in polythene bags sealed and labelled. Synthesis of zeolites was done using hydrothermal method of synthesis adopted from Ref. [16] with the clay samples as source of silica and alumina. The clays were each calcined at 600 °C for 2 h. The calcined clays were mixed with 2 M NaOH solutions and aged for 24 h before crystallization in an electrical oven at 105 °C. The samples were then washed with distilled water until the pH was less than 9. The as-synthesized zeolites from the different clay sources MK, AB and ANF were dried at 60 °C under vacuum, sieved to obtain a uniform particle size (particles retained on 180 μMesh) and labelled MZ, ABZ and ANFZ respectively.

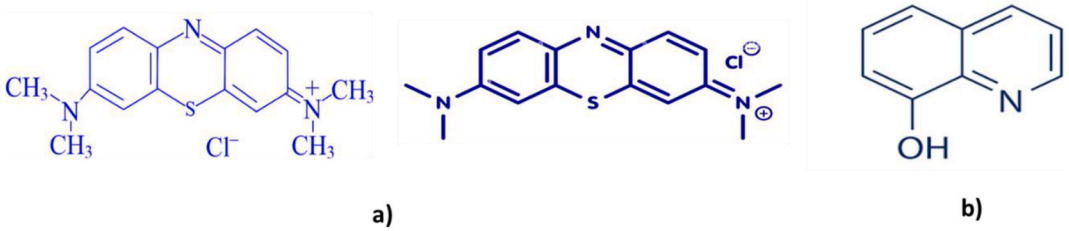

Fig. 1. Resonance structures of a) MB and b) 8-HQ.

3.2. Characterization of the adsorbents

Bulk elemental composition of the adsorbents was studied using the Olympus X-ray Fluorescence (XRF) analyser (VMR -Olympus Vanta M Series, USA). A Bruker Tensor 27 Fourier Transform Infrared (FTIR) spectrometer equipped with a golden gate Attenuated Total Reflectance (ATR) sample cell was also used to study the bond structure and interactions present between the dyes and the as-synthesized zeolites. The spectrum was obtained at a resolution of 4 cm^{-1} over the range of 500–4000 cm^{-1}. Scanning Electron Microscopy/Energy Dispersion X-ray (SEM/EDX), ZEISS EVO50 equipment, was used to study the surface morphology (size and shape) of the as-synthesized zeolites and the elemental composition of the micro-sized zeolitic materials. X-ray Diffraction (XRD) analyses were conducted using a Bruker D2 Phaser model. The scans were taken from $2\theta = 5^{\circ}$ to 76.057° with a continuous scan of step size 0.010° from a radiation source of wavelength ($\lambda = 1.5406$ Å). The crystallite sizes of the zeolites were determined using the Scherrer formula, according to the following equation (1):

$$D = \frac{K\lambda}{\beta \cos\theta} \tag{1}$$

where λ is the wavelength of the x-ray, K is the Scherrer constant, D is crystallite size at FWHM (full width at half maximum).

3.3. Adsorption study

3.3.1. Kinetic studies

About 0.4 g of zeolite was weighed into a 500 ml conical flask and recorded to 0.1 mg 200 ml of 0.03799 mol/l of MB was added and shook continuously using a Thermo Scientific MAXQ 4450 mechanical shaker whilst maintaining a laboratory temperature of 25 °C 5 ml aliquots of the mixture were taken at 5 min' intervals for 200 min and filtered through a Whatman No. 1 filter paper. The concentration of the dye in the filtrate was determined using the Agilent Cary 60 UV Vis spectrophotometer at a maximum absorbance wavelength of 610 nm. The time at which the concentration of the dyes in solution does not significantly change was taken as the equilibrium.

3.3.2. Adsorption isotherm studies

About 0.2 g each of sample was weighed into conical flasks and recorded to 0.1 mg. Six (6) aqueous solutions of pH 3.97 and 6.25 for MB and 8HQ respectively with concentrations ranging between 0.02 and 0.3 mol/l were prepared. The adsorbents were mixed with 100 ml of solution at different concentrations and maintained at laboratory temperature of 25 °C whilst shaking for 20 min at which time equilibrium is reached. The pH of the solutions at equilibrium (t = 20 min) were 9.03 for MB and 8.64 for 8HQ. The mixture was then filtered through a Whatman No. 1 filter paper and the concentration of the adsorbate was determined using the Agilent Cary 60 UV Vis spectrophotometer at a maximum absorbance wavelength of 610 nm for MB and 320 nm for 8-HQ.

The effect of the initial MB concentrations was investigated. 1 g of each zeolite was mixed with 100 ml ml of aqueous solutions, containing various initial concentrations of MB (0.02–3.140 mmol/l) for a period of 0–240 min. The equilibrium concentrations (Ce) were recorded.

Experimental data from adsorption processes are often modelled with adsorption isotherms to identify the accuracy of the theoretical assumptions using linear regression analysis tools. This helps in quantifying the distribution of the adsorbates on the adsorbent. The accuracy of the predictions with coefficient of determination (R^2) closer to unity are indicative of the consistency of the adsorption isotherm. This study considered three adsorption isotherms to predict and quantify the adsorption phenomenon at the surface of the zeolitic materials.

The Langmuir Isotherm has been used to predict a monolayer adsorption of dyes at the interface. It assumes a balance of the relative rates of adsorption and desorption to achieve surface coverage. A linearized equation of the Langmuir model is given by equation (2):

$$C_e/q_e = \frac{1}{q_{max}K} + \frac{C_e}{q_{max}} \tag{2}$$

where C_e is the concentration of adsorbate at equilibrium (in solution), K is the Langmuir constant, q_e is the equilibrium concentration of adsorbate on the adsorbent and q_{max} is the maximum adsorption capacity (mg/g).

The Freundlich Isotherm assumes surface heterogeneity and the exponential distribution of active adsorptive sites. A linearized equation (see Eqn. (3)) of the Freundlich model is given by:

$$log\ q_e = \log K_f + \frac{1}{n_f} log\ C_e \tag{3}$$

where, K_f is the adsorption capacity and $1/n_f$ is the adsorption intensity.

The Temkin Isotherm model assumes the effects of indirect adsorbate/adsorbate interactions on the adsorption process and that the heat of adsorption of all molecules at the interface decreases linearly as a result of increased surface coverage. A linearized equation of the Temkin isotherm is:

$$q_e = \frac{RT}{b}\ln K_T + \frac{RT}{b} ln\ C_e \tag{4}$$

where b is Temkin constant related to the heat of sorption, R is the universal gas constant, T is the absolute temperature and K_T is the Temkin Isotherm Constant as expressed in equation (4).

The Halsey Isotherm is used to evaluate multilayer adsorption at a relatively larger distance from the surface. It is indicative of a heteroporous nature of the adsorbent. A linearized equation of the Halsey isotherm is represented by equation (5) below:

$$log\ q_e = \frac{1}{n_H} ln\ K_H - \frac{1}{n_H} ln\ C_e \tag{5}$$

where K_H and n_H are Halsey isotherm constants.

4. Results & discussions

4.1. Elemental analysis of the adsorbents

The hydrothermal synthesis method used to prepare the zeolites from parent clays directly produces zeolites with different range of SiO_2/Al_2O_3. XRF analysis of the parent clay AB, MK and ANF showed a SiO_2/Al_2O_3 ratio of 1.47, 2.42 and 3.81 respectively. Since the mass ratio of SiO_2/Al_2O_3 of zeolites are usually greater than one, the parent clays composition of SiO_2 and Al_2O_3 are ideal for synthesis of low silica zeolites which are more hydrophilic. The EDAX analysis of the as-synthesized zeolites from the different clay sources (Table 1) indicates a low Silica/Alumina mass ratio for the zeolites synthesized as MZ (1.05), ABZ (1.06) and ANFZ (2.50) [14]. The transformation of clay into zeolites was successful given the Si/Al mass ratio. The Si/Al ratio of approximately 1:1 (for both MZ and ABZ) suggests that zeolite LTA was synthesized. This was confirmed by the XRD analysis. The Si/Al ratio of ANFZ was relatively higher ratio of 2.2:1 indicating a substitution of Al^{3+} by Si^{4+} in the zeolite framework. Zeolite Y was obtained from the ANF clay. A further elucidation of the Si/Al ratio of zeolite framework structure was done using XRD to define the dimensions of the channels and hence its classification as small (ring diameter 2.8–4 Å), medium (ring diameter 5–6 Å), or large (ring diameter >7 Å) pore zeolites.

4.2. XRD analysis of as-synthesized zeolitic materials

Sharp peaks indicating crystalline samples were observed at $2\theta = 7.18°$, 10.17°, 12.48°, 16.11°, 21.67° and 23.98° for zeolites synthesized from AB and MK clays as shown in Fig. 2a–b. These peaks correspond to theoretical zeolite LTA [17]. The crystallite size (sub grain size of the zeolite material from the XRD analysis) as determined from the Scherrer's Equation (Eqn. (1)) was 10.40 nm and 9.24 nm for ABZ and MZ respectively. Zeolites synthesized from ANF portrayed peaks (Fig. 2c) at $2\theta = 6.12°$, 10.00°, 11.78°, 15.43°, 23.33°, 26.65° and 29.2°. Similar peaks were reported by Refs. [17,18] confirming the FAU type zeolites. Slight shifts in peak positions could be attributed to the presence of certain elements (dopants) and variation of the crystallographic lattice plane distances within the zeolite framework [19,20].

4.3. Morphological characterization of adsorbents by SEM

SEM micrographs give information on the homogenity or otherwise and the morphology (size and shape) of the particles. The SEM images of the synthesized zeolites (Fig. 3a–b) show cubic well defined structures depicting zeolite LTA with (mean ± SD) particle diameter of 1.6 ± 0.3 μm and 0.84 ± 0.12 μm for ABZ and MZ respectively. The size of MZ was statistically different from that of ABZ. Similar morphologies were reported by [16]. ANFZ, however show hexagonal shaped crystals (Fig. 3c), characteristic of FAU type zeolite Y [21,22] with (mean ± SD) particle diameter of 0.88 ± 0.14 μm. The particle size of the ANFZ (determined using the SEM) was not significantly different from MZ. The hexagonal shape of ANFZ suggests that the crystal will have higher surface area with more active sites for adsorption arising from a larger number of surface atoms with reduced coordination from fewer neighbouring atoms situated at corners and edges compared with the cubic crystals of MZ of similar particle diameter [23].

Table 1
Elemental oxide composition of as-synthesized zeolites using EDAX.

Mineral Composition	As- synthesized Zeolite		
	MZ	ABZ	ANFZ
Al_2O_3 (% wt/wt)	28.15	30.41	15.50
SiO_2 (% wt/wt))	29.52	32.30	38.72
Na_2O (% wt/wt)	17.66	19.01	13.08
ZnO (% wt/wt)	2.24	1.87	–
K_2O (% wt/wt)	–	–	1.33
Fe_2O_3 (% wt/wt)	–	–	4.00
MgO (% wt/wt)	–	–	1.99
TiO (% wt/wt)	–	–	2.00
LOI (% wt/wt)	22.44	19.5	23.40
SiO_2/Al_2O_3	1.048668	1.062151	2.498065

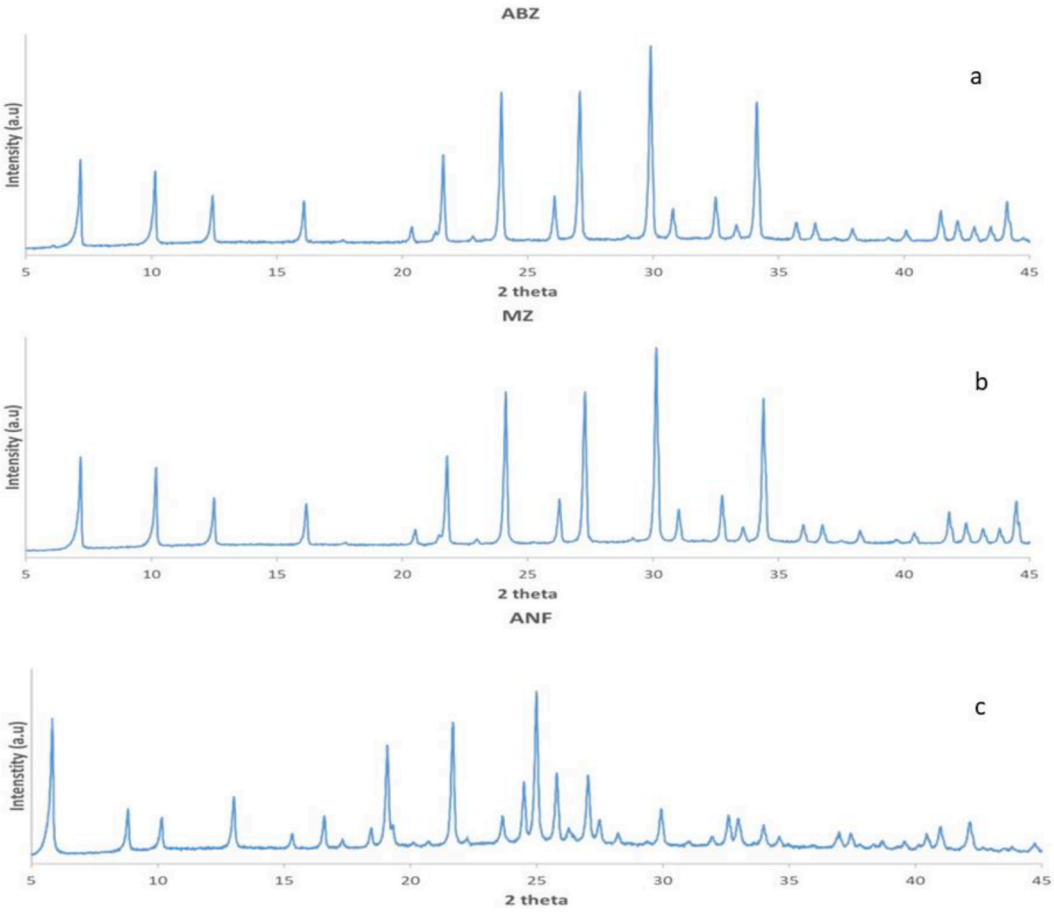

Fig. 2. XRD images of zeolites synthesized from (a) AB (b) MK and (c) ANF.

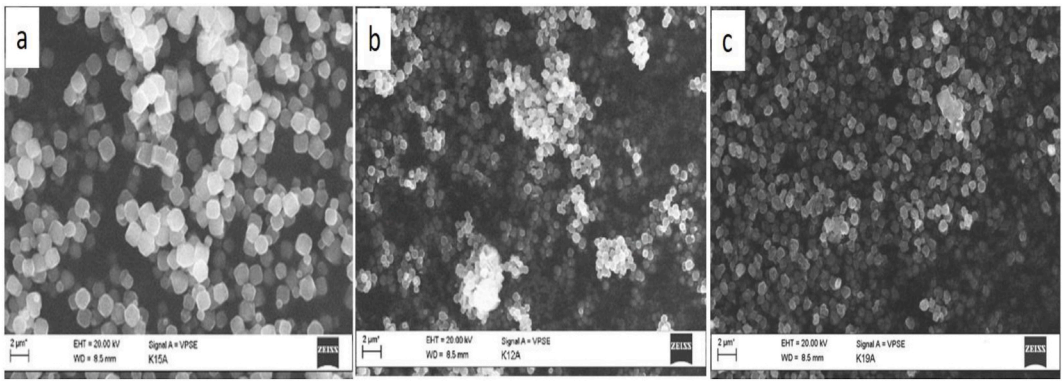

Fig. 3. Scanning electron micrograph at 20 kV beam energy and magnification bar 2 μm of the as-synthesized zeolites a) ABZ, b) MZ and c) ANFZ.

4.4. Characterization of adsorbents with FTIR spectroscopy

The fingerprint region of the absorption bands of the zeolitic materials (Fig. 4) shows absorption bands at 918 cm^{-1} and 1294 cm^{-1} which are in the range of quartz absorption bands with 1294 cm^{-1} indicating a cyclic stretching of *Si*–O. The Al–O band for aluminosilicates is observed at 761 cm^{-1} for each of the zeolites synthesized with the different clays. Bands due to pseudo-lattice vibrations are found in the region 500–800 cm^{-1}. These vibrations are insensitive to the nature of the channel cations, as well as to the Si/Al ratio [24]. The functional group region of the FTIR of the zeolitic materials synthesized (Fig. 4) show weak broad peak (3200 - 2700 cm^{-1}) indicative O–H stretching of an intramolecular bond of adsorbed water molecules and the usual bending vibration of water at 1625

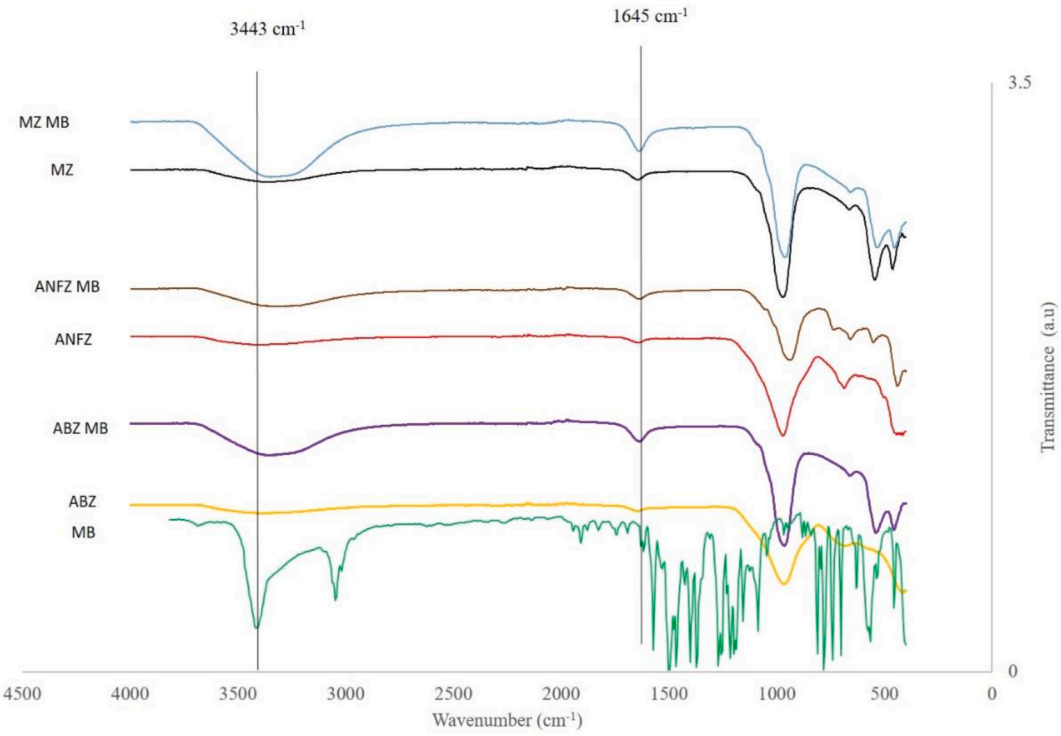

Fig. 4. FTIR spectra of the as-synthesized zeolitic materials from different clay sources, reference MB and MB adsorbed on the zeolites ABZ, ANFZ and MZ.

cm^{-1} [25]. The weak peak between 2600 and 2550 cm^{-1} is typical of S–H stretching of a thiol which could have been adsorbed from atmosphere.

4.5. Adsorption studies of MB and 8-HQ on zeolites

4.5.1. Kinetics of the adsorption of methylene blue on zeolites

From the kinetic studies as shown in Fig. 5, the adsorption of MB on the ANFZ using a solid to liquid ratio of 1:500 shows that after 15 min, the concentration of the dye in solution does not change significantly. This suggests the attainment of saturation and the optimum adsorption capacity of the zeolite. Thus, the 20 min was considered long enough to reach a dynamic equilibrium between

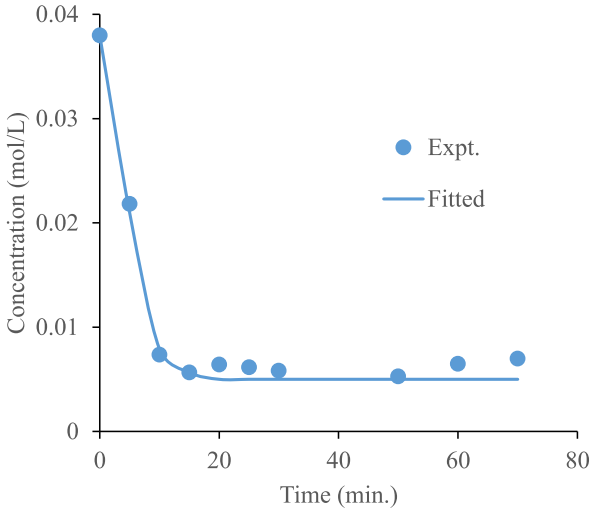

Fig. 5. Kinetics of the adsorption of MB dyes on ANFZ at 25 °C.

concentration of the adsorbate in solution and on the surface of the adsorbent.

4.5.2. Methylene blue on zeolites

The equilibrium adsorption plots on MB removal by the as-synthesized zeolites at room temperature is presented in Fig. 6. The adsorption equilibrium is established between the adsorbed molecules and the adsorbent surface when an adsorbate is in contact with the adsorbent. Fig. 6 shows significant adsorption of MB at low concentrations by all the zeolites. The mechanism of action which exists between the adsorbent surface and adsorbate can be described as a multilayer adsorption.

The adsorption profile of MB, with TPSA 43.9 $Å^2$, computed by Cactvs 3.4.8.18 [26] best fits into a Freundlich isotherm model with a Standard Error of the Regression (0.01) showing a high precision of the prediction and a coefficient of determination (R^2) greater than 99% (Fig. 8, 8a2 & 8a3 and Table 2). This indicates surface heterogeneity in terms of plane, edge and corner atoms responsible for the adsorption process for all the zeolite materials, FAU and LTA. There was significant difference ($p < 0.05$) between the adsorption capacity of FAU (ANFZ, 79.34 mg/g) and LTA (MZ, 77.07 mg/g and ABZ, 76.44 mg/g) however, there was no significant difference between adsorption on the LTA zeolites (Fig. 9) despite significant differences in size and for that matter surface area. The significant difference between adsorption of MB, a cationic dye on FAU and LTA is informative of the active sites responsible for the adsorption on the structural framework of FAU. The geometry of an adsorbed particle is assumed to be responsible for some mass transfer mechanisms [27]. This attests to the influence of geometric factors (crystal shape) in the adsorption of MB on the as-synthesized zeolites. There is a higher number of corner and edge atoms (relatively larger surface area) on the hexagonal structure of zeolite FAU (ANFZ) as seen in the micrograph (Fig. 3c) compared to the cubic structure of zeolite LTA (MZ) of similar size. The higher surface area of FAU (ANFZ) depicted by the smaller crystallite size (5.6 nm from XRD) as compared to MZ (9.2 nm) and ABZ (10.4 nm) has also been corroborated in earlier work [23].

The near perfect fit of the adsorption process to a Halsey isotherm ($0.997 < R^2 \leq 1$) demonstrates the influence of indirect adsorbate/adsorbate interactions on subsequent adsorption unto the surface and a multilayer adsorption at a relatively larger distance from the surface of the adsorbent (Fig. 1010a1, 10a2 and 10a3). The Halsey's equilibrium constant (K_H) of MB was between 0.674 and 0.679 whilst n_H ranged between 2.27 and 2.32 for the zeolites used in the study. Earlier study using acid-conditioned zeolite surfaces however, for the removal of Cu reported K_H and n_H of 1.074 and 0.351 respectively [29]. Table 2 shows the adsorption capacities of various adsorbents and adsorbates similar to this study in literature.

The Temkin adsorption isotherm model (Fig. S1) with a Standard Error of Regression of 0.22 ($0.55 < R^2 < 0.98$) and the Temkin constant K_T of MB on the different zeolites ranged from 33.57 mg/g to 48.96 mg/g (Table 2) which was higher than adsorption of MB on 40 μm natural zeolites reported in earlier work [34]. The presence of other metals in the characteristic negatively charged zeolite lattice framework, because of cation exchange, has been shown to influence surface affinity of the adsorbates on the zeolite [35]. Electronic effect influence greater affinity to cationic dyes due to the more negative polar centres at the surface of ANFZ because of the higher Si/Al ratio as well back-donation from the d-orbitals of transition elements in the zeolitic framework (see Table 1). However, since the negative charges on the LTA (MZ and ABZ) are very similar because of similar cation exchange levels (Table 1) as well as having similar crystal geometry (shape, cubic and crystallite sizes of 10.4 nm and 9.2 nm which may not be significantly different), the difference in adsorption capacities of MB on the LTA zeolites are not statistically significant (MZ, 77.07 mg/g and ABZ, 76.44 mg/g). Thus, after geometric factors influenced the initial adsorption at the surface electronic factors influence the next layers of adsorption quite remote from the surface of the adsorbent. Similar adsorption capacities were observed for the removal of basic blue 9 (MB) using erionite and clinoptilolite zeolites [36]. The study reported values of 88 mg/g and 82 mg/g for equilibrium reached after 72 h (Table 2). The maximum MB adsorption efficiency using Clin/Fe_3O_4 (97.57%) and Alg/Clin/Fe_3O_4 (93.62%) were obtained at an initial pH of 10 followed a Langmuir isotherm model [37].

4.5.3. 8-HQ on zeolites

Fig. 7 shows the adsorption mechanism of 8-HQ removal by the zeolites at equilibrium concentrations. A multilayer interaction is observed between the adsorbent and adsobate.

Similarly, the adsorption of 8-HQ. a zwitterionic molecule with smaller TPSA (33.1 $Å^2$) [6] as compared to MB (TPSA 43.9 $Å^2$) on

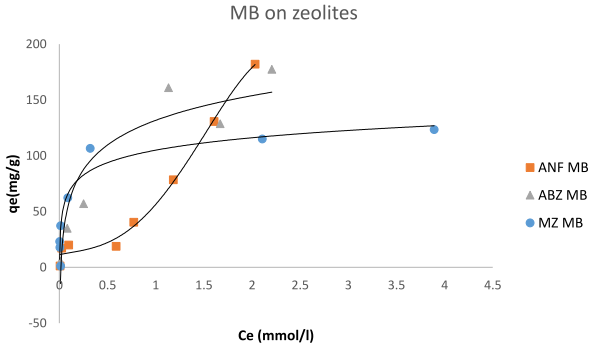

Fig. 6. Equilibrium adsorption plots of MB on the as-synthesized zeolites.

Table 2
Adsorptive capacities of various adsorbents and adsorbates.

Adsorbent	Dye	Adsorption capacity	Reference
ZK	MB	21.41	[28]
ZSM-5	MB	8.67	[4]
Erionite	MB	88 mg/g	[29]
Zeolite	Everzol red 3BS	111.1 g/kg	[30]
Activated carbon (cotton)	MB	180 mg/g	[30]
Zeolite LTA	MB	3.9 mg/g	[31]
Sodalite octahydrate zeolite	MB	3.5 mg/g	[31]
Activated Carbon	HQ	30.582 mg/l	[32]
Activated Carbon (shea residue)	HQ	45.02 mg/g	[32]
Fe-GAC	HQ	24.47 mg/g	[33]

all the as-produced zeolitic materials showed that 99% of the experimental values fitted the Freundlich Isotherm model with a standard error of about 0.02 (Fig. 8b1, 8b2 & 8b3 and Table 2). The accurate fitting to the Freundlich (Fig. 8) and Halsey Isotherms (Fig. 10b1, 10b2 and 10b3) confirm the heterogeneity of the surfaces of the zeolitic materials synthesized as well as a multilayer adsorption process. The adsorption capacities for 8-HQ on zeolite LTA (32.93 mg/g, 33.48 mg/g for ABZ and MZ respectively) and 33.61 mg/g for zeolite FAU (ANFZ) were not significantly different (Fig. 11). They were, however, unexpectedly lower than the adsorption of MB on all the zeolite types studied given the smaller TPSA of 8-HQ. This could be explained by the electrostatic repulsion of the negative centre of the zwitterionic 8-HQ molecule away from the negatively charged zeolite surface. This limits surface coverage to only adsorption based on electrostatic attraction between the positive centre of the 8-HQ and the negatively charged zeolite surface (electronic factors) [38]. The Halsey equilibrium constant for the adsorption of 8-HQ on the zeolites (K_H = 0.743–0.749) was significantly greater than that of MB (Table 3) which could imply that, the initial adsorption process is favoured for the smaller molecule. However, subsequent adsorption is limited through electronic repulsion resulting in lower maximum adsorption capacity.

4.6. FTIR studies on the adsorption of dyes on zeolitic surfaces

The FTIR absorption band of strong intensity for Ar–H (3100-2900 cm^{-1}), medium intensity C]N (*ca* 1600 cm^{-1}) and the C–N stretching (1200-1350 cm^{-1}) indicates the adsorption pattern typical of MB and 8-HQ dyes (Fig. 4). Thus, characteristics of the FTIR spectra about these unique bands is indicative of the dye's covalent bonding unto the surface of the zeolite material. Characteristically the = C–H stretching of the aromatic ring of both MB and 8-HQ (3000 cm^{-1}- 2800 cm^{-1}) is not indicated when the dye is adsorbed unto the zeolite. This shows the affinity of the aromatic centres for covalent bonding with the zeolite surface. The presence of C]N stretching band at 1635 cm^{-1} shows a repulsion of the nucleophilic amine functional group from the surface of the zeolitic material (Fig. 4). This elucidates the structural orientation of the dye molecule as it approaches the surface of the zeolite inferring electronic influences in the adsorption mechanism.

The characteristic first order reflection peak observed at $2\theta = 7.11^{\circ}$ typical of zeolite LTA, saw a gradual shift and reduction in intensity of the peak in the diffractograms of zeolites ABZ and MZ after dye adsorption (Fig. 12). This displacement is an indication of the presence of compounds (dyes) with low crystallinity present within the pores of the zeolite crystals as the d spacing value was found to increase for zeolite LTA type (MZ and ABZ) as shown in Table 4. Similar observation has been reported [1] with an increase in basal spacing with the adsorption of basic red dye on bentonite. The shift in 2 theta diffraction peaks as shown in Fig. 12 is a result of compressive stress because of the adsorption of the dyes which affects the internal properties (lattice parameters) of the crystalline adsorbent. The shift is more prominent in LTA zeolites than the FAU zeolites. The large distortion in the internal properties of the LTA zeolites compared to FAU zeolites on adsorption of the dyes could explain why the adsorption capacity is lowered in LTA adsorbents when a larger dye molecule is placed on it.

The crystal structure of zeolites is generally determined by the oxygen number and pore formation. Adsorption characteristics of zeolites are known to be influenced by pore size (formed by the arrangement of atoms with planar distances), basicity, electric field strength due to the presence of cations [39]. Due to the relatively larger distances between the lattice planes (d-spacing) of zeolite FAU (ANFZ) compared with LTA (ABZ and MZ) as well as their small crystallite size (Table 3), ANFZ will have higher surface area for the adsorption of dye molecules (MB). The pore aperture of FAU formed by the 12 membered oxygen rings provide a larger free diameter

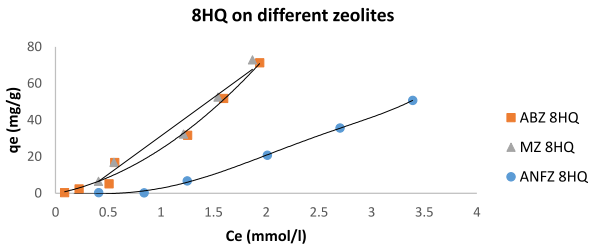

Fig. 7. Equilibrium adsorption plots of 8-HQ on the as-synthesized zeolites.

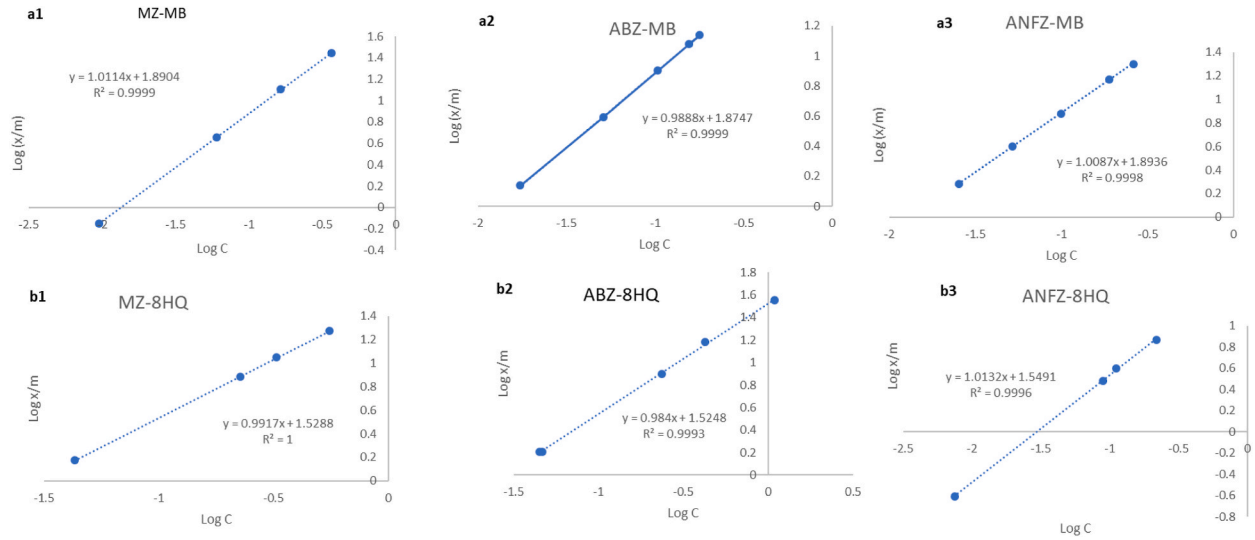

Fig. 8. Adsorption of MB on (a1) MZ, (a2) ABZ, (a3) ANFZ and 8-HQ on (b1) MZ, (b2) ABZ, (b3) ANFZ zeolite materials modelled on a Freundlich isotherm at 25 °C.

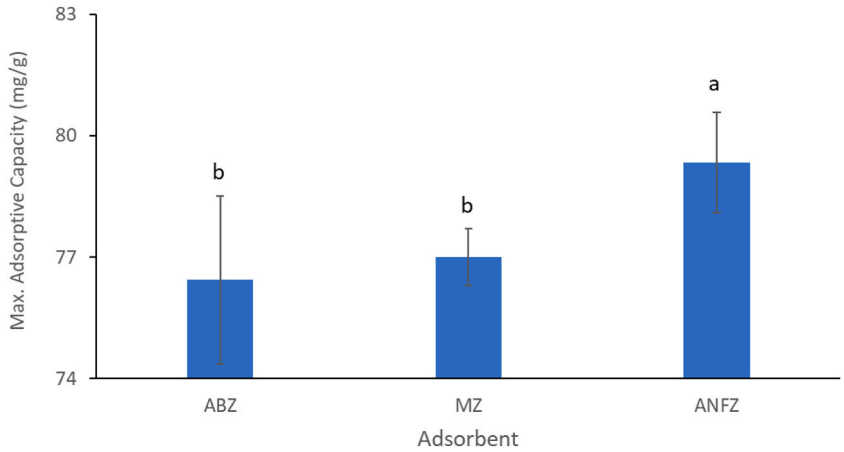

Fig. 9. The adsorption capacities of the as-synthesized adsorbents of MB from aqueous solution using different adsorbents at 25 °C.

(7.4 Å * 7.4 Å) compared with that of LTA with 8 membered rings (4.1 Å * 4.1 Å).

FAU and LTA zeolites both show sensitivity to stress in the internal structure leading to cell shrinkage as a dye is adsorbed, as shown in Fig. 12 with the shift towards larger angles. The shrinkage is higher in LTA than FAU. This significant reduction in internal surface area of LTA could cause steric hindrance on adsorption of first few molecules which also explains the lower adsorption capacity of the LTA zeolites.

FAU zeolite (ANFZ) showed more sensitivity to the type of adsorbent (MB or 8-HQ). This is because most of the electrophilic centres of the zeolite has been occupied by metal ions present in the parent clay during synthesis. The back donation of electrons from the d-orbital metals (Fe, Zn) within the zeolite structure changes the zeolite surface electronically from electrophilic to nucleophilic hence electrostatically repelling the electron rich sites of 8-HQ.

Steric hindrances occasioned by molecular orientation at the surface has been reported to be influenced by electronic factors by limiting the sticking probability of the adsorbate [40]. The electronic effect of metals in the lattice structure significantly reduce the adsorption capacity of 8-HQ, dyes with smaller TPSA, on zeolite FAU making it have similar adsorption capacities as LTA. Thus, it can be deduced that adsorption of dyes on zeolitic materials are driven by both geometric and electronic considerations. However, it would be necessary to perform Ar adsorption-desorption studies to prove the geometric effects conclusively.

5. Conclusions

The formation of zeolites LTA or FAU during hydrothermal synthesis from local deposits of clay is dependent on the Si/Al ratio of

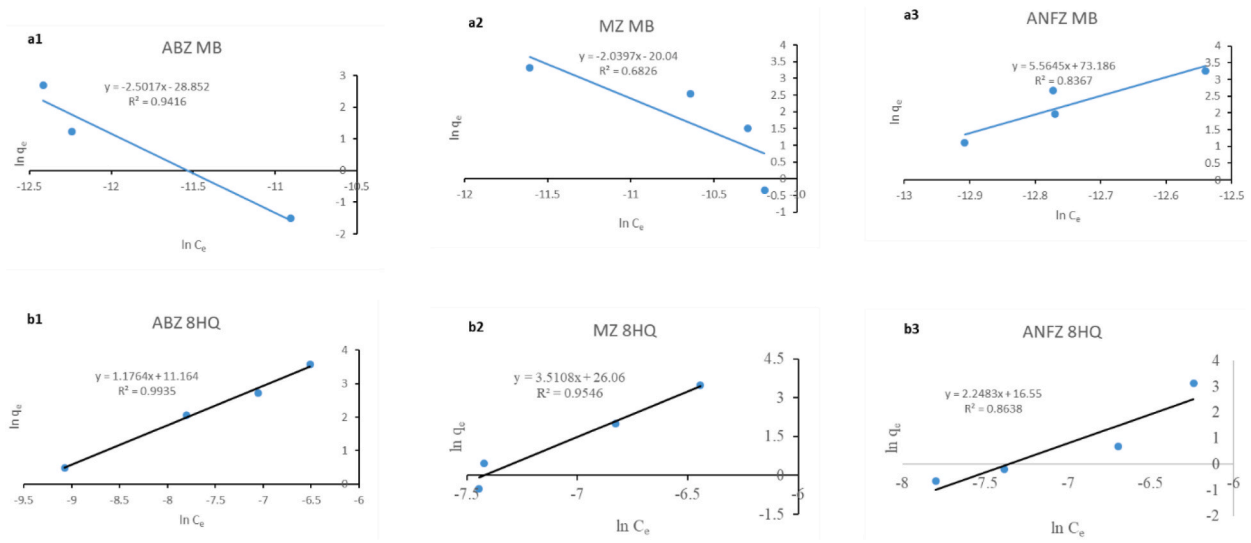

Fig. 10. Adsorption of MB on (a1) ABZ, (a2) MZ, (a3) ANFZ and 8-HQ on (b1) ABZ, (b2) MZ, (b3) ANFZ zeolite materials modelled on a Halsey isotherm at 25 °C.

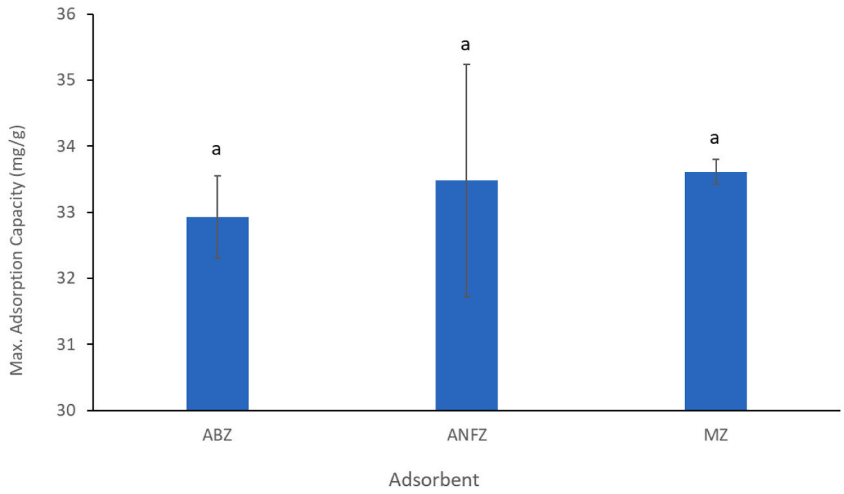

Fig. 11. The adsorption capacities of the as-synthesized zeolites of 8-HQ from aqueous solution using different adsorbents at 25 °C.

the precursor clay. The ensuing zeolitic materials exhibit properties which influenced the adsorption characteristics of cationic and zwitterionic dyes in aqueous solutions. The adsorption of the dyes modelled a Freundlich isotherm. The optimum adsorption capacities at 20 min for the as-produced ABZ and MZ (zeolites LTA) by methylene blue were 76.44 mg/g and 77.07 mg/g respectively which were significantly lower than ANFZ (Zeolite FAU), 79.43 mg/g. However, there is no significant difference in the adsorption capacities of both Zeolite LTA and FAU when removing 8-hydroxyquinoline from a pH 8.64 solution (32.93 mg/g, 33.46 and 33.61 mg/g for ABZ, MZ and ANFZ respectively). Both XRD and FTIR techniques depicted the presence of the adsorbates on the adsorbents and the subsequent interactions were found to be driven by both geometric (inter lattice spacing which imparts higher surface area of the adsorbent) and electronic (electrostatic repulsions through electron back donation from metals in the zeolitic structure) considerations.

Author contribution statement

Elizabeth Von-Kiti: Conceived and designed the experiments; Performed the experiments; Analyzed and interpreted the data; Contributed reagents, materials, analysis tools or data; Wrote the paper. William Owusu Oduro: Conceived and designed the experiments; Analyzed and interpreted the data; Wrote the paper. Maame Adwoa Bentumah Animpong: Performed the experiments; Analyzed and interpreted the data. Kofi Ampomah Benefo: Performed the experiments; Analyzed and interpreted the data; Wrote the

Table 3
Adsorption Isotherm models for MB and 8-HQ from aqueous solution using different zeolites at 25 °C.

Zeolite - Dye	Isotherm	Constants		
		q_{max}	R_L	R^2
MZ-8HQ	Langmuir	0.7499	0.9691	0.9695
ANFZ-8HQ		0.3214	0.9310	0.6791
ABZ-8HQ		0.5012	0.9535	0.6051
ANFZ- MB		0.1760	0.7662	0.9130
MZ - MB		0.9547	0.9495	0.7724
ABZ MB		0.9732	0.9503	0.3589
		b	K_T	R^2
MZ-8HQ	Temkin	397365.9	24.4522	0.8751
ANFZ -8HQ		526941.7	60.8673	0.8589
ABZ -8HQ		252492.9	23.2390	0.9110
ANFZ - MB		288563.3	38.2008	0.8944
MZ - MB		440714.9	48.9554	0.9353
ABZ - MB		327558.4	33.5660	0.9476
		n_H	K_H	R^2
MZ-8HQ	Halsey	2.3218	0.7462	1.0000
ANFZ -8HQ		2.3036	0.7432	1.0000
ABZ -8HQ		2.3397	0.7485	0.9993
ANFZ - MB		2.2686	0.6748	0.9972
MZ - MB		2.3170	0.6791	1.0000
ABZ- MB		2.3004	0.6743	0.9995
		n_f	K_f	R^2
MZ-8HQ	Freundlich	1.0084	33.7909	0.9989
ANFZ -8HQ		0.9870	35.4079	0.9990
ABZ-8 HQ		1.0163	33.4811	0.9988
ANFZ- MB		0.9914	78.2708	0.9992
MZ- MB		0.9862	77.6962	0.9995
ABZ- MB		1.0113	74.9376	0.9998

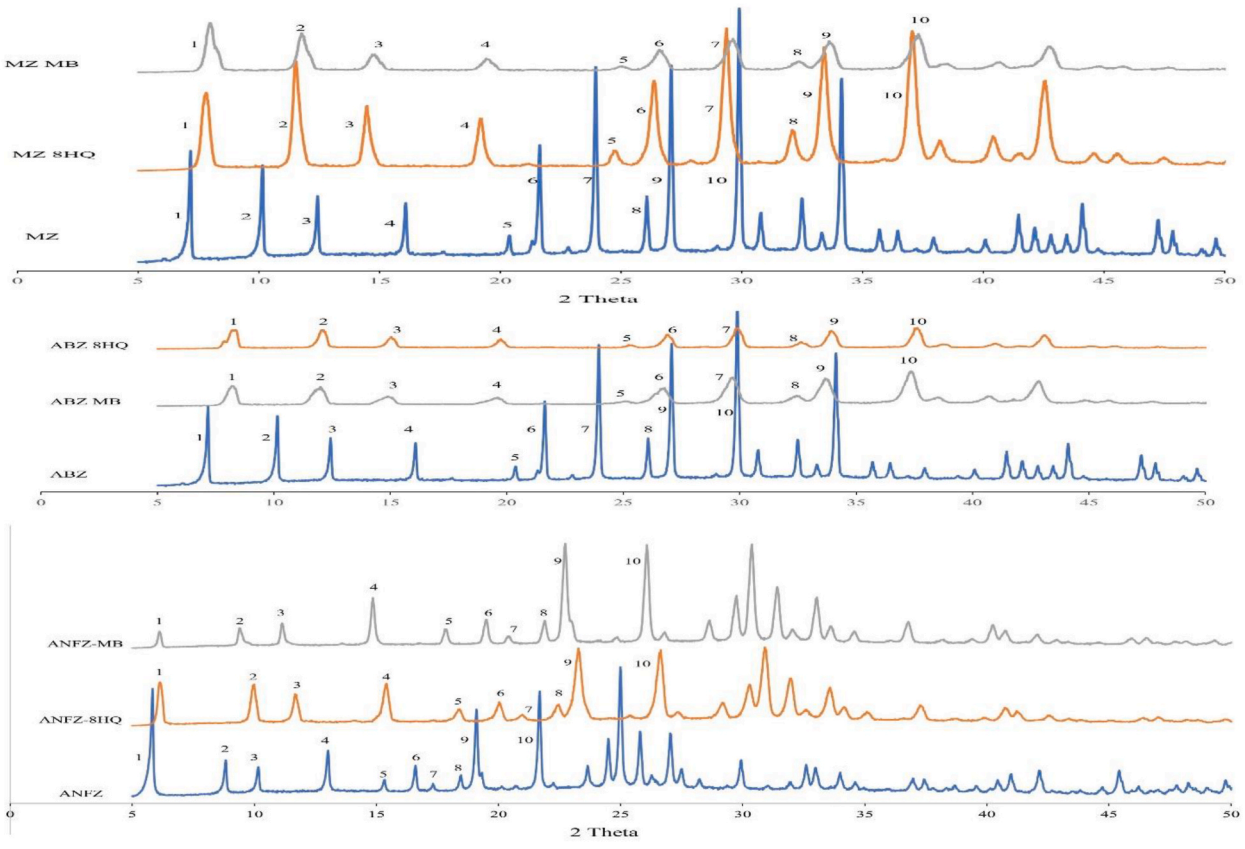

Fig. 12. Peak displacements of the individual zeolites, with peaks labelled numerically 1–10, before and after adsorption of 8-HQ and MB.

Table 4
Diffraction angle (2θ) and its corresponding d-spacing of the zeolites before and after adsorption of the dyes.

Zeolite Type	Adsorbent	2θ Miller indices (111)	d spacing
LTA	ABZ	7.166	12.326
	ABZ MB	7.300	12.342
	ABZ HQ	7.190	12.332
	MZ	7.141	12.370
	MZ MB	7.295	12.240
	MZ HQ	7.173	12.340
FAU	ANFZ	6.085	14.513
	ANF MB	6.115	14.360
	ANF HQ	6.126	14.450

paper. Gloria Boafo-Mensah: Performed the experiments; Contributed reagents, materials, analysis tools or data. Bright Kwakye-Awuah: Conceived and designed the experiments; Wrote the paper. Craig Denver Williams: Conceived and designed the experiments; Contributed reagents, materials, analysis tools or data; Wrote the paper.

Data availability statement

Data will be made available on request.

Declaration of competing interest

The authors declare that they have no known competing financial interests or personal relationships that could have appeared to influence the work reported in this paper.

Acknowledgement

This project was funded by the Royal Society Leverhulme-Africa Postdoctoral award (LAF/R1/180020).

Appendix A. Supplementary data

Supplementary data to this article can be found online at https://doi.org/10.1016/j.heliyon.2023.e20049.

References

[1] Q.H. Hu, S.Z. Qiao, F. Haghseresht, M. Wilson, Adsorption study for removal of basic red dye using bentonite, Ind. Eng. Chem. Res. 45 (2) (2006) 733–738.
[2] O. Ozdemir, B. Armagan, M. Turan, M.S. Celik, Comparison of the adsorption characteristics of azo-reactive dyes on mesoporous minerals, Dyes Pigments 62 (2004) 49–60.
[3] M. Rakanović, A. Vukojević, M.M. Savanović, S. Armaković, S. Pelemiš, F. Živić, S. Sladojević, S.J. Armaković, Zeolites as adsorbents and photocatalysts for removal of dyes from the aqueous environment, Molecules 27 (19) (2022) 6582.
[4] G. Oprea, A. Michnea, C. Mihali, Adsorption kinetic of 8-hydroxyquinoline on malachite, Am. J. Appl. Sci. 4 (8) (2007) 592–596.
[5] B. Erdem, A. Özcan, S.A. Özcan, Adsorption and solid phase extraction of 8-hydroxyquinoline from aqueous solutions by using natural bentonite, Appl. Surf. Sci. 256 (17) (2010) 5422–5427.
[6] National Center for Biotechnology Information, Compound Summary for CID 1923, 8-Hydroxyquinoline, PubChem ., 2023.
[7] A.A. Ajibola, I.O. Adeoye, B.O. Solomon, Adsorption of dyes using different types of clay: a review, Appl. Water Sci. 7 (2) (2017) 543–568.
[8] B. Alica, L. Blinová, M. Sirotiak, A. Michalíková, Usage of FTIR-ATR as non-destructive analysis of selected toxic dyes, Research Papers Faculty of Materials Science and Technology Slovak University of Technology 25 (40) (2017) 103–111.
[9] R.K. Vital, K.N. Saibaba, K.B. Shaik, R. Gopinath, Dye removal by adsorption: a review, J. Biorem. Biodegrad. 7 (6) (2016) 1–4.
[10] M.N. Rashed, Adsorption technique for the removal of organic pollutants from water and wastewater, in: M.N. Rashed (Ed.), Organic Pollutants: Monitoring, Risk and Treatment, Rijeka, InTech, 2013, pp. 167–178.
[11] L. Deng, Q. Xu, H. Wu, Synthesis of Zeolite-like Material by Hydrothermal and Fusion Methods Using Municipal Solid Waste Fly Ash, Procedia Environmental Sciences, 2016, pp. 662–667.
[12] S.A. Kovo, M.O. Edoga, Production and Characterization of Zeolite from Ahako Clay in Kogi State, Nigeria, Leonardo Electronic Journal of Practices and Technologies, 2005, pp. 31–40.
[13] K. Ramesh, D.D. Reddy, Zeolites and their potential uses in agriculture, Adv. Agron. 113 (2011) 219–241.
[14] C. Wang, S. Leng, H. Guo, J. Yu, W. Li, L. Cao, J. Huang, Quantitative arrangement of Si/Al ratio of natural zeolites using acid treatment, Appl. Surf. Sci. 498 (2019), 143874.
[15] D. Kalló, Applications of natural zeolites in water and wastewater treatment, Rev. Mineral. Geochem. (2001) 519–550.
[16] B. Kwakye-Awuah, E. Von-Kiti, R. Buamah, I. Nkrumah, C. Williams, Effect of Crystallization Time on the Hydrothermal Synthesis of Zeolites from Kaolin and Bauxite, IJSER, 2014, pp. 734–741.
[17] M.M. Treacy, J.B. Higgins, Collection of Simulated XRD Powder Patterns for Zeolites, fifth ed., Elsevier., Netherlands, 2007.
[18] H. Ramezani, S.N. Azizi, G. Cravotto, Improved Removal of Methylene Blue on Modified Hierarchical Zeolite Y: Achieved by a "Destructive-constructive" Method, Green Processing and Synthesis, 2019, pp. 730–741.
[19] B.R. Kumar, B. Hymavathi, X-ray peak profile analysis of solid-state sintered alumina doped zinc oxide ceramics by Williamson-Hall and size-strain plot method, Journal of Asian Ceramic Societies 5 (2) (2017) 94–103.

[20] Z.Y. Li, W.M. Lam, C. Yang, B. Xu, G.X. Ni, S.A. Abbah, K.M. Cheung, K.D. Luk, W.W. Lu, Chemical composition, crystal size and lattice structural changes after incorporation of strontium into biomimetric apatite, Biomaterials 28 (7) (2007) 1452–1460.
[21] O.O. Ltaief, P.C.S. Siffert, S. Fourmentin, M. Benzina, Optimal synthesis of faujasite-type zeolites with a hierarchical porosity from natural clay, Eur. J. Inorg. Chem. 28 (2015) 4658–4665.
[22] N. Salahudeen, Ahmed, S. A, Synthesis of hexagonal zeolite Y from Kankara kaolin using a split technique, J. Inclusion Phenom. Macrocycl. Chem. 87 (2017) 149–156.
[23] D. Guaya, C. Hernan, J. Camacho, C.M. Lopez, C. Valderrama, J.L. Cortina, LTA and FAU-X Iron-enriched zeolites: use for phosphate removal from aqueous medium, Materials 15 (15) (2022) 5418.
[24] B. Cansever, Treatment of Domestic Wastewater with Natural Zeolites, MSc Thesis," Izmir Institute of Technology Izmir, Turkey, 2004.
[25] B.C. Erdogan, Cr (VI) Removal with Natural, Surfactant Modified and Bacteria Loaded Zeolites. PhD Dissertation, Izmir Institute of Technology, Turkey, 2011.
[26] National Center for Biotechnology Information, Compound Summary for CID 6099, Methylene Blue, PubChem, 2023.
[27] P.S. Pauletto, G.L. Dotto, N.P.G. Salau, P.S. Pauletto, Dotto, Diffusion mechanisms and effect of adsorbent geometry on heavy metal adsorption.,", Chem. Eng. Res. Des. 157 (2020) 182–194.
[28] D.M. El-Mekkawi, F.A. Ibrahim, M.M. Selim, Removal of methylene blue from water using zeolites prepared from Egyptian kaolins collected from different sources, J. Environ. Chem. Eng. 4 (2) (2016) 1417–1422.
[29] A.A. Abin-Bazaine, L.M. Rodríguez-Vázquez, E. Santellano-Estrada, S. Rodríguez-Piñeros, L. Cortés-Palacios, Copper removal by acid-conditioned zeolite, Part I: equilibrium, and numerical simulations, J. Environ. Earth Sci. 9 (3) (2019) 2224–3216.
[30] M.N. Rashed, Adsorption technique for the removal of organic pollutants from water and wastewater, in: Organic Pollutants-Monitoring, Risk and Treatment, 2013, pp. 167–194.
[31] M.T. Asefa, G.B. Feyisa, Comparative investigation on two synthesizing methods of zeolites for removal of methylene blue from aqueous solution, Int. J. Chem. Eng. 2022 (2022).
[32] A.L. Adoum, T. Kamgaing, R.F.T. Tagne, C.D. Atemkeng, I.-H.T. Kuete, o.G. Anagho, Optimized removal of hydroquinone and resorcinol by activated carbon based on shea residue (Vitellaria paradoxa): thermodynamics, adsorption mechanism, J. Chem. 2022 (2022) 1–12.
[33] A. Tyagi, S. Das, V.C. Srivastava, Tyagi, Ankit, Susmita DasRemoval of toxic hydroquinone: comparative studies on use of iron impregnated granular activated carbon as an adsorbent and catalyst, Environmental Engineering Research 24 (3) (2019) 474–483.
[34] A.B.D. Nandiyanto, S.N. Hofifah, S. Anggraeni, T. Kurniwan, Isotherm adsorption of 40-μm zeolite particles for treatment of dye wastewater, J. Eng. Sci. Technol. 17 (2) (2022) 1265–1275.
[35] M. Tatlier, C. Atalay-Oral, A. Bayrak, T. Maras, A. Erdem, Impact of ion exchange on zeolite hydrophilicity/hydrophobicity monitored by water capacity using thermal analysis, Thermochimica 713 (2022), 179240.
[36] V. Hernández-Montoya, M. Pérez-Cruz, D. Mendoza-Castillo, M. Moreno-Virgen, A. Bonilla-Petriciolet, Competitive adsorption of dyes and heavy metals on zeolitic structures, J. Environ. Manag. 116 (2013) 213–221.
[37] M. Noori, M. Tahmasebpoor, R. Foroutan, M. Noori, M. Tahmasebpoor, Forout, Enhanced adsorption capacity of low-cost magnetic clinoptilolite powders/beads for the effective removal of methylene blue: adsorption and desorption studies.,", Mater. Chem. Phys. 278 (2022), 125655.
[38] B. Erdem, A. Ozcan, S.A. Ozcan, Adsorption and solid phase extraction of 8-hydroxyquinoline from aqueous solutions by using natural bentonite, Appl. Surf. Sci. 256 (17) (2010) 5422–5427.
[39] M.J. Regufe, A.M. Ribeiro, A.F. Ferreira, A. Rodrigues, "CO2 storage on zeolites and other adsorbents, in: Nanoporous Materials for Gas Storage, Springer, Singapore, 2019, pp. 359–381.
[40] W.O. Oduro, N. Cailuo, K.K. Yu, H. Yang, S.C.E. Tsang, Geometric and electronic effects on hydrogenation of cinnamaldehyde over unsupported Pt-based nano-crystals, Journal of Physical Chemistry Chemical Physics 13 (7) (2011) 2590–2602.